Materials for Energy
Workshop "Advances in Fuel Cells and Hydrogen"
April 2010, Torres Vedras, Portugal

PERFORMANCE OF A SOLAR-HYDROGEN STAND-ALONE SYSTEM FOR RESIDENTIAL APPLICATIONS

P.J.R. PINTO*, C.M. RANGEL*

Laboratório Nacional de Energia e Geologia (LNEG), Fuel Cells and Hydrogen Unit,
Estrada do Paço do Lumiar 22, 1649-038 Lisboa, Portugal
*paulo.pinto@lneg.pt; *carmen.rangel@lneg.pt

ABSTRACT: Hydrogen, as an energy storage medium, is considered a promising solution to overcome the limitation of intermittent renewable energy sources. In this paper, a residential scale solar-hydrogen based stand-alone energy system is designed, modelled and the simulated system performance under real end-use load, representative of standard European domestic electrical energy consumption, and meteorological conditions is analyzed. The sun is the primary energy source of the system and a fuel cell-electrolyzer combination is used as a backup and a long-term storage system. A battery bank is also used as energy buffer and for short time storage. Matlab/Simulink® is used for the overall system modelling and simulation. The results show that the designed solar-hydrogen system is in principle capable of operating autonomously and in a sustainable manner. The designed system is able to convert 7.6% of the total energy irradiated in one year.

Keywords: Solar hydrogen, stand-alone system, modelling, energy management, system sizing.

RESUMO: O hidrogénio, como um meio de armazenamento de energia, é considerado uma solução promissora para superar a limitação da intermitencia das fontes de energia renováveis. Neste trabalho é dimensionado e modelado um sistema de energia solar-hidrogénio isolado da rede de distribuição de energia eléctrica e à escala residencial. São analisados os resultados da simulação do seu desempenho sob condições climatéricas e de carga, esta última representativa do padrão de consumo de energia eléctrica no sector residencial na Europa. O sol é a fonte primária de energia do sistema e uma combinação pilha de combustível-electrolisador é usada como um sistema de apoio e como um sistema de armazenamento de longo prazo. É também usado um banco de baterias como reserva de energia e de armazenamento de curto prazo. O Matlab / Simulink® é utilizado para a modelação e simulação de todo o sistema. Os resultados mostram que o sistema solar-hidrogénio projetado é, em princípio, capaz de operar autonomamente e de forma sustentável. O sistema projectado é capaz de converter 7,6% do total de energia irradiada num ano.

Palavras chave: Hidrogénio solar, sistema autónomo, modelação, gestão de energia, dimensionamento do sistema.

NOMENCLATURE

Acronyms

AC	alternating current
DC	direct current
MPPT	maximum power point tracker
PEMFC	proton exchange membrane fuel cell
PHOEBUS	PHOtovoltaik-Elektrolyse-Brennstoffzelle Und Systecknik
PV	photovoltaic
RE	renewable energy

Symbols

A	area (m²)
B	slope of Tafel line (V)
C	equivalent capacitance (F)
D	constant in the mass transfer term (V)
DoA	days of autonomy
DoD	depth of discharge
E	energy (kWh)
f_1	parameter related to Faraday efficiency (mA²cm⁻⁴)
f_2	parameter related to Faraday efficiency
I, i	current (A)

K	thermal correction factor ($\Omega°C^{-1}$)
M	number of moles (mol)
MH	metal hydride
n	diode quality factor
N	number of cells or modules
P	power (W)
r	parameter related to ohmic resistance of electrolyte (Ωm^2)
R	resistance (Ω)
s	coefficient for overvoltage on electrodes (V)
t	coefficient for overvoltage on electrodes ($A^{-1}m^2$)
T	temperature (°C)
U, u	voltage (V)
V	volume (m^3)
$\dot{n}\,n$	molar flow rate ($mol\,s^{-1}$)
α	ratio between the current irradiance and the irradiance at standard rating conditions
η	efficiency

Subscripts

BAT	battery bank
BUS	DC-bus
$BUS-BAT$	from DC-bus to battery bank
$BUS-EZ$	from DC-bus to electrolyzer
$BUS-EZ\_MAX$	electrolyzer maximum input seen from the DC-bus
$BUS-EZ\_MIN$	electrolyzer minimum input seen from the DC-bus
$BUS-LOAD$	from DC-bus to end-use load
$CELL$	cell
DAI	daily average solar irradiation
DAL	daily average end-use load
EZ	electrolyzer
EZR	electrolyzer rated
EZ_EL	electrolyzer electrode
EZ_H2	hydrogen produced by the electrolyzer
EZ_OFF	limit for electrolyzer operation
EZ_ON	level to activate electrolyzer
EZ_REF	electrolyzer reference
EZ_R	electrolyzer reversible
F	Faraday
FC	fuel cell
FCR	fuel cell rated
$FC-BUS$	from fuel cell to DC-bus
$FC-BUS\_MAX$	fuel cell maximum output seen from the DC-bus
FC_H2	hydrogen consumed by the fuel cell
FC_L	fuel cell limiting
FC_N	fuel cell internal
FC_O	fuel cell exchange
FC_OFF	limit for fuel cell operation
FC_ON	level to activate fuel cell
FC_REF	fuel cell reference
FC_R	fuel cell reversible
M	membrane and contact
MAI	month average solar irradiation
MAL	month average end-use load
MAX	maximum acceptable

MH	metal hydride
MH_I	initial hydrogen content in the metal hydride
MH_T	total hydrogen capacity in the metal hydride
MIN	minimum acceptable
NET	production minus consumption
PV	photovoltaic
$PV-BUS$	from photovoltaic array to DC-bus
PV_L	photocurrent
PV_MIN0	minimum initial photovoltaic array
PV_MIN1	minimum photovoltaic array
PV_O	photovoltaic module reverse saturation
PV_STC	photovoltaic module electrical values under standard test conditions
REF	at standard rating conditions
S	series
SH	shunt
SOC	state of charge
SOC_MAX	maximum state of charge
SOC_MIN	minimum state of charge
YAI	yearly average solar irradiation

Constants

F	Faraday constant ($F=96485\,C\,mol^{-1}$)
LHV	low heating value of hydrogen ($LHV=3\,kWh\,m^{-3}$)
z	number of electrons transferred per reaction ($z=2$

1. INTRODUCTION

The combined effect of the rising prices of fossil fuels and the growing awareness of the impact of environmental pollution has stimulated great interest in alternative and clean energy sources, such as solar and wind. They produce little or no environmental pollution, are unlimited and available almost everywhere on the earth. However, their inherent intermittency and variability renders storage of energy indispensable for fitting time-varying load demand.

A hydrogen system comprising a hydrogen producing unit (electrolyzer), a hydrogen storage unit and a hydrogen utilizing unit (fuel cell) is considered a promising solution for renewable energy storage. Compared to commonly used battery storage, hydrogen storage has higher storage density and lesser environmental effect. During the past decade, the interest on the concept of integrating renewable energy sources with hydrogen storage systems for stand-alone applications has increased. Experimental results of prototype or actual systems have been reported by several researchers [1-6] focusing on system performance and viability. Many simulation studies focusing on system energy management and control strategies [7-10], sizing [11-15] and modeling [16-19] are also available in the literature.

The integrated system unit-sizing and energy flow control are two major research challenges because of their interdependence, the temporal mismatch between energy supply and demand, the non-linear characteristics of the individual units of the system and the high number of variables and param-

eters. To properly size the integrated system units, research-ers [11,12] used the "yearly average monthly" method in which the unit-sizing is conducted by considering the yearly averaged monthly values of meteorological and load demand data. When the goal is to find the optimum unit-size and/or the control strategy for the integrated system, researchers [13-15]used time-series simulation coupled with optimiza-tion methods. In most studies, the energy flow is controlled through the state of charge of the battery bank, which is com-monly used for short-term energy storage. Due to their inher-ent characteristics (poor dynamic response of fuel cells and intermittent nature of RE sources), stand-alone RE hydrogen systems must include a short-term response energy storage device.

The focus of this paper is to examine the performance of a stand-alone solar-hydrogen system for residential applica-tions in terms of the final amount of hydrogen in the storage unit, the level of utilization and operating pattern of battery bank, electrolyzer and fuel cell. Starting with a description of the system to be investigated, the dynamic model of each unit is briefly described. The major equations are provided and the key model parameters are given. Simulation results obtained using Matlab/Simulink® are then presented and analyzed.

2. SYSTEM DESCRIPTION

2.1. Configuration

Fig. 1 shows the schematic diagram of the considered system, which consists of a photovoltaic (PV) array for solar energy conversion, an alkaline water electrolyzer for hydrogen pro-duction, a metal-hydride for hydrogen storage, a proton ex-change membrane fuel cell (PEMFC) for hydrogen energy conversion and a battery bank for energy buffering. All the units are linked via a common DC-bus, which allows energy to be managed between sources, storages and end-use load. The battery bank is directly connected to the DC-bus, while the PV generator, the electrolyzer and the PEMFC are cou-pled to the DC-bus via boost-based maximum power point tracker (MPPT), buck and boost converters, respectively. The end-use load is powered by the DC-bus through a DC-AC converter (inverter).
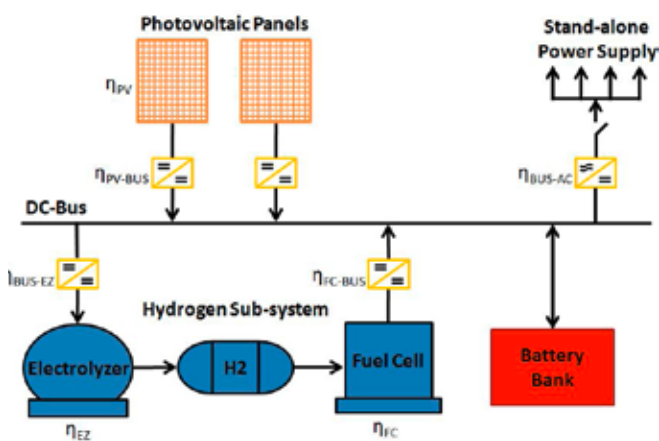

Fig. 1. Layout of the considered solar-hydrogen stand-alone system.

2.2. Energy management and control strategy

The main requirements of the designed energy management strategy for the stand-alone solar-hydrogen system are to sat-isfy the end-use load under variable meteorological condi-tions and to manage the energy flow while ensuring efficient operation of the different system units. The PV-generated en-ergy is primarily used to meet the end-use load. Any excess of energy is used to charge the battery bank or to produce hydrogen through water electrolysis. Any shortage of energy is met by the PEMFC and/or the battery bank. The inherent variability in the solar generation produces variability in the operation of the PEMFC and the water electrolyzer. Since sta-ble operation of these energy systems is vital for efficiency, lifetime and cost, the management strategy uses the battery bank to mitigate the effects of energy fluctuations on their operating pattern. In this implementation, a double hysteresis loop control strategy is used for this purpose, see Fig. 2. The on/off switching actions of the PEMFC and the water electro-lyzer are determined by DC-bus voltage, u_{BUS}, where U_{EZ_ON}, U_{EZ_OFF}, U_{FC_ON} and U_{FC_OFF} are the key decision parameters.
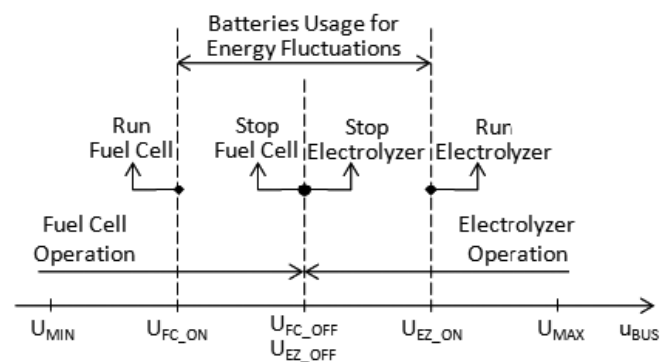

Fig. 2. Representation of the operation of the considered solar-hydrogen stand-alone system.

To apply the energy management strategy easily, all quanti-ties of the energy conversion units (PV array, PEMFC and water electrolyzer) and the end-use load are referred into the DC-bus by taking the losses associated with the power con-version units into consideration. Control flow is shown in Fig. 3 and is based on the following instantaneous current balance equation at the DC-bus:

$$i_{NET} = i_{BUS\text{-}EZ} - i_{FC\text{-}BUS} \pm i_{BUS\text{-}BAT} \text{ (A)} \tag{1}$$

where i_{NET} is the PV-generated current, $i_{PV\text{-}BUS}$, minus the end-use load current, $i_{BUS\text{-}LOAD}$.

Basically, at any given time, any excess PV-generated energy ($i_{NET} > 0$) is supplied to the battery bank to charge it or to the water electrolyzer to produce hydrogen. The electrolyzer is activated when $MH_{SOC} < MH_{SOC\_MAX}$, $u_{BUS} >= U_{EZ\_ON}$ and $i_{NET} >= I_{BUS\text{-}EZ\_MIN}$ (a minimum electrolyzer threshold input current has been assigned for safety reasons). If $0 < i_{NET} < I_{BUS\text{-}EZ\_MIN}$ and in the previous time step the electrolyzer was operating, then the electrolyzer is not disconnected and the deficit current, $i_{NET} - I_{BUS\text{-}EZ\_MIN}$, is provided by the battery bank. On the other hand, if $i_{NET} > I_{BUS\text{-}EZ\_MAX}$, then the electrolyzer utilizes current equal to $I_{BUS\text{-}EZ\_MAX}$ and the surplus current, $i_{NET} - I_{BUS\text{-}EZ\_MAX}$, is used to charge the battery bank without exceeding U_{MAX}
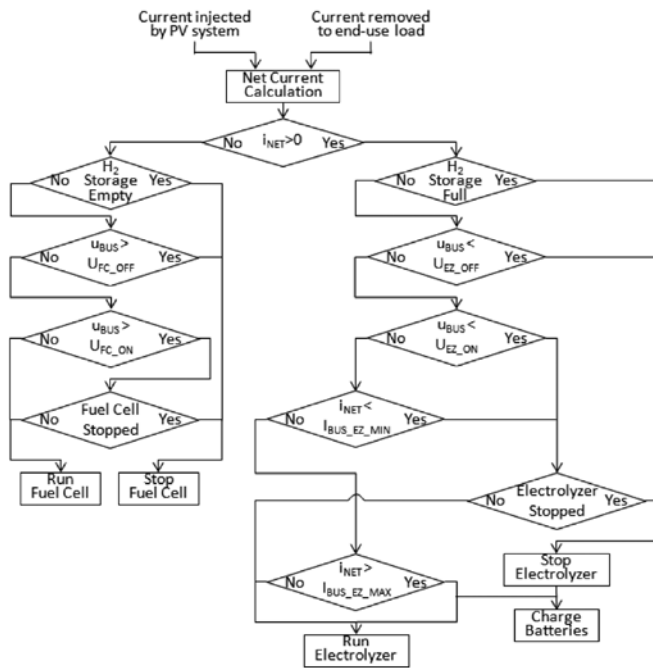
Fig. 3. Control logic flow chart.

to avoid overcharging. The electrolyzer on/off state from the previous time step is maintained unaltered for $U_{EZ\_OFF} <= u_{BUS} < U_{EZ\_ON}$.

When there is a deficit in PV-generated energy ($i_{NET} < 0$), the deficit is covered by the battery bank and/or the PEMFC. The PEMFC is activated when $MH_{SOC} > MH_{SOC\_MIN}$ and $u_{BUS} <= U_{FC\_ON}$. If $|i_{NET}| < I_{FC-BUS\_MAX}$, then the PEMFC is set to provide the deficit current and to charge the battery bank without exceeding its charging current limit. On the other hand, if $|i_{NET}| > I_{FC-BUS\_MAX}$, then the remaining current deficit is covered by the battery bank. The PEMFC on/off state from the previous time step is maintained unaltered for $U_{FC\_ON} < u_{BUS} <= U_{FC\_OFF}$.

In the range $U_{FC\_ON} < u_{BUS} < U_{EZ\_ON}$ and provided that neither the electrolyzer nor the PEMFC are operating, the battery bank is charged ($i_{NET} > 0$) or discharged ($i_{NET} < 0$) depending on the net current level.

2.3. Unit-Sizing

The solar-hydrogen stand-alone system is assumed to be installed in a house located near Lisbon, Portugal (Lat.: 38.84; Long.: -9.12). Local hourly averaged solar irradiation intensity on a surface tilted at 38.8 degrees and ambient temperature profiles are used for modeling the performance of the PV generator. These data are derived from the measured data available in Ref. [20]. The end-use load is taken from Ref. [21] and it represents standard European domestic electrical energy consumption. The data is from a mother and two children dwelling, averaged over a 5 minute time interval. The monthly averaged solar irradiation on the tilted plane and end-use load energies for the time period spanned by the simulation run (one year) are shown in Fig. 4. The key data are listed in Table 1.
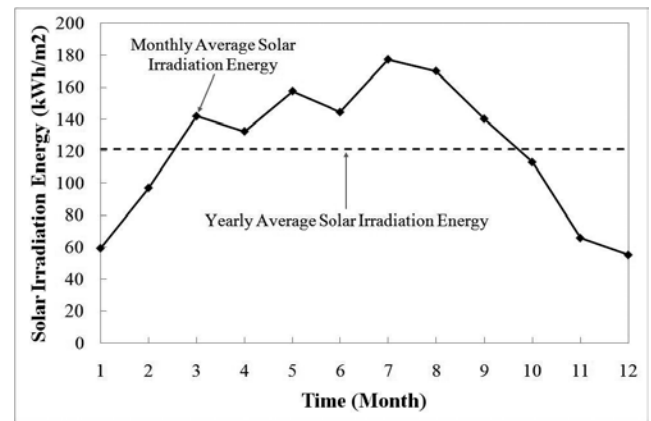
(a)
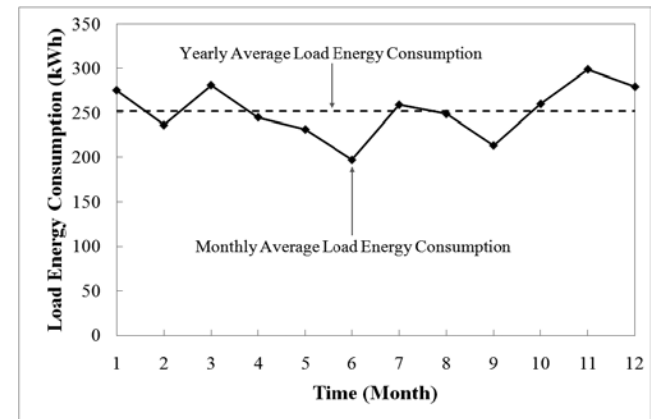
(b)

Fig. 4. Monthly averaged (a) solar irradiation on the tilted plane and (b) end-use load energies.

Table 1. End-use load and solar irradiation.

End-use load	
Daily average energy E_{DAL} (kWhday^{-1})	8
Yearly average energy (kWhm^{-2} per year)	252
Total energy consumption (kWh)	3029
Solar irradiation	
Daily average energy E_{DAI} (kWhday^{-1})	4
Yearly average energy E_{YAI} (kWhm^{-2} per year)	121
Total energy usable (kWhm^{-2})	1453

Based on the designed energy management strategy and on the yearly solar irradiation and end-use load energies profiles just characterized, the following unit-sizing procedure is used to determine the size of the battery bank, the PEMFC, the PV array, the alkaline water electrolyzer and the metal-hydride. In this study, the assumed efficiencies of the main system units are as follows: battery bank (η_{BAT}), 85%; PEMFC (η_{FC}), 35%; PV array (η_{PV}), 14%; alkaline water electrolyzer (η_{EZ}), 75%; DC-DC converters (η_{PV-BUS}, η_{BUS-EZ} and η_{FC-BUS}), 95%; DC-AC converter ($\eta_{BUS-LOAD}$), 90%.

The battery bank energy capacity E_{BAT} is determined by:

$$E_{BAT} = \frac{E_{DAL}}{\eta_{BUS-LOAD}\eta_{BAT}} \frac{DoA}{DoD} (kWh)$$

(2)

where E_{DAL} is the daily average end-use load energy (kWhday^{-1}), DoA is the days of autonomy (one day of autonomy

is considered here) and *DoD* is the depth of discharge of the battery bank (U_{EZ_ON}-U_{FC_ON} in this case).

The PEMFC is also sized for the daily average end-use load energy and its rated power is determined by:

$$P_{FCR} = \frac{E_{DAL}}{\eta_{BUS-LOAD}\eta_{FC-BUS}24h}(W)$$

(3)

A safety margin of 25% is added to the calculated values of the battery bank energy capacity and the PEMFC rated power.

The PV array size is determined through the following steps:

- In order to assure the autonomy of the system, the daily average end-use load energy must come directly from the PV array. Hence, the minimum initial area of the PV array is determined by:

$$A_{PV\_MIND} = \frac{E_{DAL}}{E_{DAI}\eta_{PV}\eta_{PV-BUS}\eta_{BUS-LOAD}}(m^2)$$

(4)

- However, due to the mismatch between energy generation and consumption, there are additional energy losses in the hydrogen loop. Based on the initial area, A_{PV_MIN0}, of the PV array, the monthly average mismatch between solar energy and end-user load energy is shown in Fig. 5. In this case, we use monthly averages to simplify the calculations. From March to September, the system produces more energy than the load demand. The excess of energy can be used to produce hydrogen. From October to February, there is a deficit of energy and the system needs to consume hydrogen in order to cover the load demand. The minimum PV array area required to accommodate the energy losses in the hydrogen loop can be calculated by:

$$A_{PV\ MIN1} = A_{PV\ MIN0} +$$

$$\frac{(1-\eta_{BUS-EZ}\eta_{EZ}\eta_{FC}\eta_{FC-BUS})}{\eta_{BUS-EZ}\eta_{EZ}\eta_{FC}\eta_{FC-BUS}12\ months} \times$$

$$\sum_{March}^{September}(E_{MAI}\eta_{PV}\eta_{PV-BUS} - E_{MAL}/\eta_{BUS-LOAD})(m^2)$$
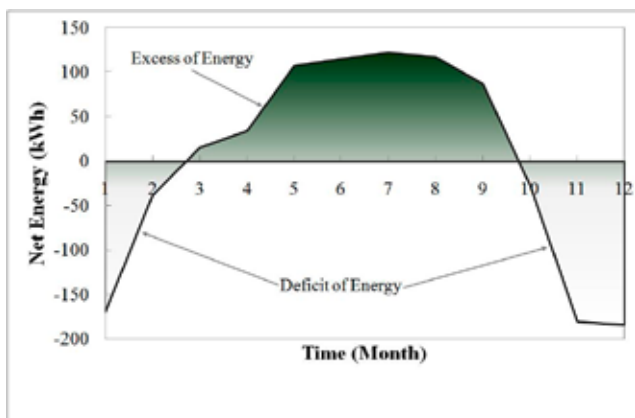
(5)

Fig. 5. PV-generated energy minus the end-use load energy (net energy), referred into the DC-bus.

The electrolyzer should be able to handle the maximal power of the PV array. The maximum possible rated power of the electrolyzer is given by:

$$P_{EZR} = N_{PV}P_{PV\ STC} - \eta_{PV-BUS}\eta_{BUS-EZ}\ (W)$$

(6)

However, due to the inherent intermittency and variability of solar irradiation, the power supplied to the electrolyzer would be below the PV maximum power output most of the time. In addition, an electrolyzer with a higher power rating means also a higher minimum operation threshold and thus lower operation time. Hence, a more economical option may be to size the electrolyzer at a power lower than the PV maximum power output (typically between 60 and 80% [15]). In this case, a percentage value of 70% is applied.

The hydrogen capacity of the metal hydride is determined by:

$$V_{MH}\frac{\eta_{BUS-EZ}\eta_{EZ}}{LHV} \times$$

$$\sum_{February}^{October}(E_{MAI}\eta_{PV}\eta_{PV-BUS} - E_{MAL}/\eta_{BUS-LOAD})(m^3)$$

(7)

where *LHV* is the lower heating value of hydrogen ($3kWhm^{-3}$). The bounds of summation in the above expression represent the months for which there is an excess of energy. These new bounds are a result of increased PV array area. In order to accommodate the metal hydride state of charge initial level and seasonal fluctuation, a factor of two is applied to the calculated value.

Following the unit-sizing procedure described in this section, the sizes of the battery bank, the PEMFC, the PV array, the alkaline water electrolyzer and the metal-hydride are estimated and listed in Table 2.

Table 2. System unit-sizing.

Battery bank	
Energy capacity E_{BAT} (kWh)	33.9
PEMFC	
Rated power P_{FCR} (W)	500
PV array	
Area A_{PV_MINI} (m^2)	27.4
Electrolyzer	
Rated power P_{EZR} (W)	2432
Metal hydride	
Hydrogen capacity V_{MH} (m^3)	1113

The PV array, battery bank and electrolyzer unit sizes used in the simulation are $28.1m^2$, 38.4kWh and 2500W, respectively. The sizes of the PV array and battery bank were chosen based on commercially available units, while the size of the electrolyzer was chosen to be a scaled-down proportion of an electrolyzer whose empirical model is reported in the literature and used in this study. The sizes of all the other units used in the simulation are those listed in the above table. Further information is contained in the next section.

3. SYSTEM'S MODEL

3.1. PV Array's and Boost-based MPPT Converter's Model

The model of the PV array refers to the electrical model with one diode. The current-voltage characteristic curve is

described by the following five-parameter implicit equation [22]:

$$i_{PV} = \alpha i_{PV\_L} - i_{PV\_0}\left(e^{\left(\alpha\left[u_{PV}+Ki_{PV}\left(T-T_{ref}\right)\right]+i_{PV}R_s\right)/anT}-1\right)$$

$$-\frac{a\left[u_{PV}+ki_{PV}\left(T-T_{ref}\right)\right]+i_{PV}R_s}{R_{sh}}(A) \qquad (8)$$

Table 3 lists the values of the empirical parameters obtained for the PV module Kyocera KC175GHT-2 [23] with a peak power of 175W in standard conditions, using the procedure reported in [22].

The maximum power output of the PV array varies with temperature and solar irradiation. Therefore, designing efficient PV systems heavily emphasizes to track the maximum power operating point. In this study, a classic perturb and observe (P&O) tracking algorithm is used involving the model of the nonlinear current-voltage characteristic of the PV module.

By taking into proper account the boost-based MPPT conversion efficiency, $\eta_{PV\text{-}BUS}$, the current to the DC-bus is given by:

$$i_{PV-BUS} = \frac{\eta_{PV-BUS}i_{PV}u_{PV}}{u_{BUS}}(A) \qquad (9)$$

Table 3. PV model parameters.

$\alpha=1$; $T=25$ºC	
I_{PV_L} (A)	8.0923
I_{PV_O} (A)	9.6024×10^{-12}
n (V/K)	3.5897×10^{-3}
R_{SH} (Ω)	99.158
R_S (Ω)	0.282
$\alpha=1$; 25-75ºC	
K (ΩºC^{-1})	1.1218×10^{-3}
$\alpha=0.2$; $T=25$ºC	
I_{PV_O} (A)	1.4356×10^{-11}

A total number of 22 modules are needed to cover the PV array area determined in the previous section (see Table 2).

3.2. Hydrogen Loop Model

Hydrogen loop is the set of units converting electrical energy into chemical energy via water electrolysis, storing it and converting it back to electrical energy by using a fuel cell.

Based on the working conditions, the energy flow controller produces a current reference for the electrolyzer or the PEMFC. Current controlled power converters could then use these current references to control the electrolyzer/PEMFC current input/output. In this study, each power converter is represented by an ideal power source where the ratio from its output power to its input power is dictated by its efficiency [8]. Hence, input/output power references can thus be determined by:

$$P_{EZ} = u_{EZ}i_{EZ} = \eta_{BUS-EZ}i_{EZ\ REF}\eta_{BUS}(W) \qquad (10)$$

$$P_{FC} = u_{FC}i_{FC} = \frac{i_{FC-REF}u_{BUS}}{\eta_{FC-BUS}}(W) \qquad (11)$$

The model of the electrolyzer is developed for a scaled-down version (2.5kW) of the PHOEBUS electrolyzer (26kW, 21 cells, 7 bar) reported in [24]. This unit is an advanced type of alkaline electrolyzer having low voltage-high current relationship. The current-voltage characteristic of the electrolyzer is expressed as:

$$\begin{cases} u_{CELL} = u_{EZ\_R} + \frac{r_1r_2T_{EZ}}{A_{EZ\_EL}}i_{EZ} + slog\left(\frac{t_1+t_2/T_{EZ}+t_3T_{EZ}^2}{A_{EZ\_EL}}i_{EZ}-1\right)(V) \\ u_{EZ} = N_{EZ}u_{CELL}(V) \end{cases} \qquad (12)$$

The values of the empirical parameters are listed in Table 4 and were obtained from measurements performed at an operating temperature of 80ºC.

The model of the PEMFC developed is based on the empirical current-voltage equation reported in [25] and is expressed as:

$$u_{FC} = u_{FC\_R} - \left(i_{FC}+i_{FC\_N}\right)R_M - B_{ln}\left(\frac{i_{FC}+i_{FC\_N}}{i_{FC\_O}}\right)$$

$$+ D\ln\left(1-\frac{i_{FC}i_{FC\_N}}{i_{FC\_L}}\right)(V) \qquad (13)$$

Table 5 lists the values of the empirical parameters obtained for a 500W PEMFC stack under a stack temperature of 55ºC, a humidifier temperature of 45ºC, and a use of hydrogen and air, respectively, of 50 and 25% at atmospheric pressure [26].

Combining equations (10) and (12) yields an expression linking the electrolyzer's current to the buck converter's output power which is solved using the Newton-Raphson method. The electrolyzer's voltage is then obtained by substituting the estimated value of the electrolyzer's current in equation (12). Similarly, from equations (11) and (13) we obtain the PEMFC operating point i_{FC}-u_{FC}. The rates of hydrogen production (electrolyzer) and consumption (PEMFC) can then be computed using the following expressions:

$$\dot{n}_{EZ\_H2} = \eta_F\frac{N_{EZ}}{zF}i_{EZ} \text{ (mols}^{-1}\text{) (Hydrogen production rate)} \qquad (14)$$

$$\dot{n}_{FC\_H2} = \frac{N_{FC}}{\eta_F ZF}i_{FC} \text{ (mols}^{-1}\text{) (Hydrogen consumption rate)} \qquad (15)$$

The Faraday efficiency of the PEMFC was assumed constant and equal to 0.9, while the Faraday efficiency of the electrolyzer is described by the following expression [24]:

$$\eta_F\frac{\left(i_{EZ}/A_{EZ\_EL}\right)^2}{f_1+\left(i_{EZ}/A_{EZ\_EL}\right)}f_2(0...1) \qquad (16)$$

Table 4. Electrolyzer model parameters [24].

A_{EZ_EL} (m²)	0.25	s (V)	0.185
f_1 (mA²cm⁻⁴)	250	t_1 (m²A⁻¹)	-1.002
f_2 (mA²cm⁻⁴)	0.96	t_2 (m²ºCA⁻¹)	8.424
N_{EZ}	2	t_3 (m²ºC²A⁻¹)	247.3
r_1 (Ωm²)	8.05×10^{-5}	u_{EZ_R} (V)	1.184
r_2 (Ωm²ºC⁻¹)	-2.5×10^{-7}		

Table 5. Fuel cell model parameters [26].

A (V)	1.35	i_o (A)	6.54×10^{-3}
B (V)	1.19	R_M (Ω)	42×10^{-3}
i_L (A)	100	u_{FC_R} (V)	27.1
i_N (A)	0.23		

The metal hydride was modeled as a simple hydrogen summation unit as described by the following expression:

$$MH_{50C} = \frac{M_{MH\_I} + J\eta_{EZ\_H2}dt - J\eta_{FC\_H2}dt}{M_{MH\_T}} (0...1) \tag{17}$$

3.3. Battery Bank Model

A simplified model of the lead-acid battery bank can be constructed by an ideal constant voltage source, U_{BAT}, in series with an equivalent internal resistance, R_{BAT}, and an equivalent capacitance, C_{BAT} [27]. Knowing the current, voltage is given by:

$$u_{BAT} = U_{BAT} + \left(i_{BAT}R_{BAT} + \frac{1}{c_{BAT}} \int i_{BAT}dt \right)\eta_{BAT} (V) \tag{18}$$

The battery bank efficiency, η_{BAT}, is considered to be equal to 0.85 (as defined in section 2.3) during charging and equal to 1 during discharging. An Autosil EE 2-800, 2V 800Ah [28], was chosen in this study as base battery for building the battery bank. Table 6 lists the values of the parameters used in the simulation for the battery bank.

Table 6. Battery bank model parameters.

Voltage source U_{BAT} (V)	42
Capacitance C_{BAT} (F)	218182
Internal resistance R_{BAT} (Ω)	1.68×10^{-3}

4. SIMULATION RESULTS

A simulation in Matlab/Simulink® environment was conducted to evaluate the performance of the solar-hydrogen stand-alone system over a one-year period under real end-use load and meteorological data. Table 6 lists the values of the control parameters used.

Table 7. System control parameters.

Electrolyzer	
Minimum input current $I_{BUS\text{-}EZ\_MIN}$ (A)	9.5
Maximum input current $I_{BUS\text{-}EZ\_MAX}$ (A)	55.7
Metal hydride	
Initial state of charge (0...1)	0.5
Minimum limit of state of charge MH_{SOC_MIN} (0...1)	0.3
Maximum limit of state of charge MH_{SOC_MAX} (0...1)	0.9
Battery bank	
Rated voltage (V)	48
Initial voltage (V)	48
Maximum charge current (A)	80
Maximum acceptable voltage level U_{MAX} (V)	55.2
Voltage level to activate the electrolyzer U_{EZ_ON} (V)	52.5
Voltage limit for electrolyzer U_{EZ_OFF} and PEMFC U_{FC_OFF} operation (V)	49.9
Voltage level to activate the PEMFC U_{FC_ON} (V)	47.3
Minimum acceptable voltage level U_{MIN} (V)	42

Figs. 6, 7 and 8 show the metal hydride state of charge correlation with the battery bank voltage, the power consumed by the electrolyzer and the power supplied by the fuel cell, respectively. We notice that, in accordance to the energy management strategy, the fluctuation in the metal hydride state of charge and the operating pattern of the battery bank, electrolyzer and PEMFC reflect the fluctuation in the system's net energy. In fact, from February to October, the system produces more energy than the load demand and thus:

- the metal hydride state of charge increases;
- the battery bank voltage fluctuates mainly between U_{EZ_OFF} and U_{EZ_ON};

- the electrolyzer operates whenever the DC-bus voltage constraint and device current limitation are satisfied;
- the PEMFC is always disconnected (except at the beginning of February, when the PEMFC is operating and the DC-bus voltage is below U_{FC_OFF}).

In contrast, from November to January, there is a deficit of energy and thus:

- the metal hydride state of charge decreases;
- the battery bank voltage fluctuates mainly between U_{FC_ON} and U_{FC_OFF};
- the electrolyzer is always disconnected;
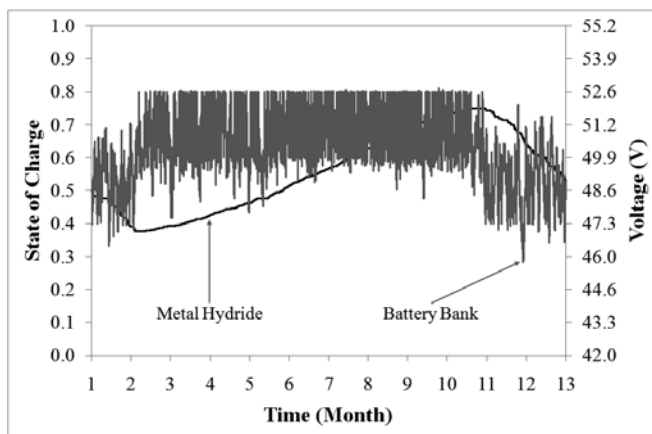- the PEMFC operates whenever the DC-bus voltage constraints are satisfied.

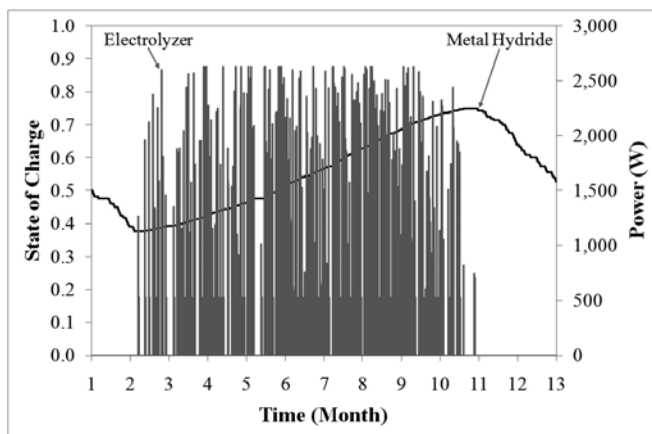**Fig. 6.** Metal hydride state of charge and battery bank voltage.

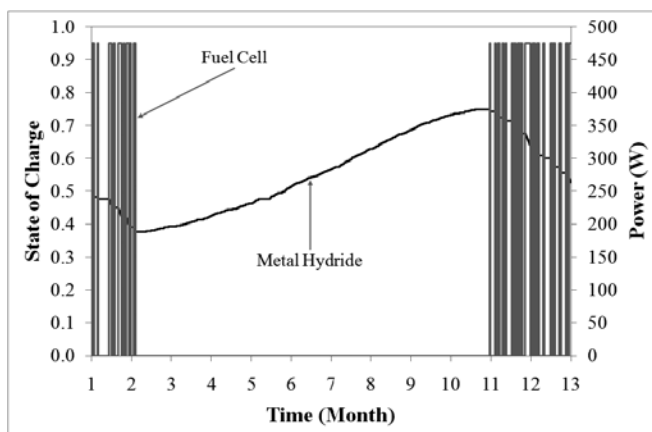**Fig. 7.** Metal hydride state of charge and power consumed by the electro-lyzer.

Fig. 8. Metal hydride state of charge and power supplied by the PEMFC.

Fig. 6 shows that the battery bank is subject to many charge-discharge partial cycles and to a long period of operation (the period of deficit of energy) at voltages below U_{EZ_ON} (i.e., the battery bank never reached a high recharging level), which shorten its lifetime. The frequency of these charge-discharge partial cycles is higher during the period of excess of energy than during the period of deficit of energy. This is due to the use of the battery bank to maintain electrolyzer operation when the net current becomes lower than the minimum electrolyzer threshold input current. Such an operating policy prolongs the duration of the electrolyzer operation after each activation, reducing the number of start and stops, which

is beneficial in terms of electrolyzer performance and life-time [7, 29]. The control of the PEMFC operation is done to achieve the same objective. Table 8 shows the performance parameters of the electrolyzer and PEMFC.

In Fig 8, it can be seen that the PEMFC operates always at rated output power. This is the result from setting the PEMFC to provide the deficit current and to charge the battery bank.

Table 8. Electrolyzer and PEMFC performance parameters.

	Electrolyzer	PEMFC
Number of starts	170	28
Minimum operating time (h)	5.1	7.7
Minimum idling time (h)	6.5	11.7
Total operating time (h)	2352.3	860.0

On an energy basis, the designed system is able to power the end-use-load continuously given the input energy available from the renewable resource. The battery bank plays an important role in maintaining the energy flows and in extending the electrolyzer operation, supplying approximately 49% of the end-use load demand and 50% of the energy consumed by the electrolyzer. But over the one year period, the system is able to keep the battery bank voltage well above the minimum acceptable limit (i.e., the system operated in a sustainable manner). The energy produced by the PV array is equal to 5.22MWh. About 29% of this energy is supplied to the end-use load, 17% is supplied to the electrolyzer and 54% is used to charge the battery bank. The relatively low percentage of energy supplied to the end-use load is due to the temporal mismatch between energy generation and consumption, which emphasizes the need for energy storage. The difference between the percentages of PV-generated energy given to the electrolyzer and to the battery bank is mainly a result of the implemented energy management strategy. In fact, only about 6% of the energy given to the battery bank is due to the constraint placed by the minimum electrolyzer current input requirement. The PEMFC provides 0.4MWh yearly energy. About 45% of this energy is given to the end-use load and 55% is given to the battery bank. The final state of charge of the metal hydride is 0.53, meaning that the system is in principle capable of operating as a stand-alone unit. 7.4% and 0.2% of the total solar irradiation are found to be supplied to the end-user and stored in the system, respectively, at the end of the testing year.

5. CONCLUSIONS

The performance of a residential scale solar-hydrogen based stand-alone energy system over a one-year period under real end-use load and meteorological conditions was analyzed by numerical simulation.

The results show that the designed system is able to service the end-use load in a sustainable manner given the input energy available from the renewable resource. Moreover, the end of period surplus hydrogen (+3%) shows that the designed system is capable of stand-alone operation. However, these

results are at the cost of an intense usage of the battery bank, which affects its life span.

There are many trade-offs between battery bank and hydrogen loop operation, depending on the energy management strategy employed. By using the current energy management strategy, the total number and magnitude of battery bank charge/discharge cycles could be reduced by, for example, narrowing the hysteresis band size. The drawbacks, however, would be an increased PEMFC operation time, an increased number of the electrolyzer start-up/stop cycles and a lower hydrogen inventory.

REFERENCES

[1]   P. Hollmuller, J. M. Joubert, B. Lachal, K. Yvon, International Journal of Hydrogen Energy 25 (2000) 97-_109.

[2]   T. K. Bose, K. Agbossou, M. Kolhe, J. Hamelin, Available online < http://www.ieahia.org/pdfs/res_uquebec.pdf>, 2004.

[3]   G. Hoffheinz, N. Kelly, A. Ete, Evaluation of hydrogen demonstration systems & United Kingdom hydrogen infrastructure (Years 2–3 of Task 18 of The IEA Hydrogen Implementing Agreement) Contract number: F/04/00287/00/Rep, URN number: 07/770, Contractor: Sgurr Energy Ltd., 2007.

[4]   J. F. Martins, A. Joyce, C. M. Rangel, J. Sotomayor, R. Castro, A. Pires, J. Carvalheiro, R. A. Silva, S. Viana, International Conference on Power Engineering, Energy and Electrical Drives, Setúbal, Portugal, 12-14 April, 2007.

[5]   H. Miland, O. Ulleberg, Solar Energy (2008), doi:10.1016/j.solener.2008.04.013.

[6]   A. Bergen, L. Pitt, A. Rowe, P. Wild, N. Djilali, Journal of Power Sources 186 (2009) 158-166.

[7]   O. Ulleberg, Solar Energy 76 (2004) 323-329.

[8]   A. Bilodeau, K. Agbossou, Journal of Power Sources 162 (2006) 757-764.

[9]   D. Ipsakis, S. Voutetakis, P. Seferlis, F. Stergiopoulos, S. Papadopoulou, C. Elmasides, Energy 33 (2008) 1537-1550.

[10]   D. Ipsakis, S. Voutetakis, P. Seferlis, F. Stergiopoulos, C. Elmasides, International Journal of Hydrogen Energy 34 (2009) 7081–7095.

[11]   C. Wang, M. H. Nehrir, IEEE Transactions on Energy Conversion 23 (3) (2008) 957-967.

[12]   K. Zhou, J. A. Ferreira, S. W.. H. de Haan, International Journal of Hydrogen Energy 33 (2008) 477-489.

[13]   C. Darras, S. Sailler, C. Thibault, M. Muselli, P. Poggi, J. C. Hoguet, S. Melscoet, E. Pinton, S. Grehant, F. Gailly, C. Turpin, S. Astier, G. Fontès, International Journal of Hydrogen Energy 35 (2010) 3322-3332.

[14]   S. Jalilzadeh, H. Kord, A. Rohani, ECTI Transactions on Electrical Eng., Electronics, and Communications 8 (1) (2010) 118-125.

[15]   P. Poggi, C. Cristofari, J. I. Canaletti, C. Darras, M. Muselli, Global Journal on Technology and Optimization (1) (2010). Available online: <http://www.pcoglobal.com/gjto.htm>.

[16]   S. S. Deshmukh, R. F. Boehm, Renewable and Sustainable Energy Reviews 12 (2007) 2301-2330.

[17]   O. C. Onar, M. Uzunoglu, M. S. Alam, Renewable Energy 34 (2009) 509-520.

[18]   M. J. Khan, M. T. Iqbal, Applied Energy 86 (2009) 2429-2442.

[19]   S. Pedrazzi, G. Sini, P. Tartarini, Energy Conversion and Management 51 (2010) 122-129.

[20]   Sistema Nacional de Informação de Recursos Hídricos, Available from: <http://snirh.pt/>.

[21]   European Electrical Specific Profiles – Annex 42, Available online: <http://www.ecbcs.org/docs/Annex_42_European_Electrical_Specifc_Profiles_Annex_42_September_2006.zip>.

[22]   V. Lo Brano, A. Orioli, G. Ciulla, A. Di Gangi, Solar Energy Materials and Solar Cells 94 (8) (2010) 1358--1370.

[23]   Kyocera KC175GHT-2 Datasheet. Available online: <http://www.kyocerasolar.eu/index/products/download/English.-cps-33141-files-16536-File.cpsdownload.tmp/KC175GHT-2_Eng_June%202007.pdf>.

[24]   O. Ulleberg, International Journal of Hydrogen Energy 28 (2003) 21-33.

[25]   J. Larminie, A. Dicks, "Fuel cell systems explained", Second ed., John Wiley & Sons, Chichester, 2003, UK.

[26]   I. Sadli, P. Thounthong, J.-P. Martin, S. Raël, B. Davat, Journal of Power Sources 156 (1) (2006) 119-125.

[27]   B. S. Borowy, Z. M. Salameh, IEEE Transactions on Energy Conversion 12 (1) (1997) 73-78.

[28]   Autosil EE 2-800 Datasheet. Available online: <http://www.autosil.pt/public/upload/PRODUTOS/BIs/BI_catalogos_tabelas/catalogo_EE.pdf>.

[29]   A. Bergen, L. Pitt, A. Rowe, P. Wild, N. Djilali, International Journal of Hydrogen Energy 34 (2009) 64-70.